Robust Tropical Tropospheric Responses to Absorbing Aerosols

GEETA PERSAD * , YI MING, AND V. RAMASWAMY

Geophysical Fluid Dynamics Laboratory/NOAA, Princeton, NJ

Corresponding author address: Geeta Persad, Geophysical Fluid Dynamics Laboratory/NOAA, 201 Forrestal Road, Princeton, NJ 08540.

E-mail: geeta.persad@noaa.gov

ABSTRACT

Absorbing aerosols affect the Earth's climate through direct radiative heating of the tropo-sphere. We analyze the Tropical tropospheric response to a globally uniform increase in black carbon, simulated with an atmospheric general circulation model, in order to gain insight into the interactions that determine the radiative flux perturbation. Over the convective regions, heating in the free troposphere hinders the vertical development of deep cumulus clouds, resulting in the detrainment of more cloudy air into the large-scale environment and stronger cloud reflection. A different mechanism operates over the subsidence regions, where heating near the boundary layer top causes a substantial reduction in low cloud amount thermodynamically by decreasing relative humidity and dynamically by lowering cloud top. These findings, which align well with previous general circulation model and large eddy sim-ulation calculations for black carbon, provide first-order physical explanations for the main characteristics of the Tropical tropospheric adjustment, suggesting that they may be robust regardless of model physics parameterization. The implications for quantifying the climate perturbation posed by absorbing aerosols are discussed.

1

1. Introduction

Absorbing aerosols (e.g. organic and black carbon) are widely considered to be potentially important contributors to global warming along with greenhouse gases (e.g. Hansen et al. 2000; Jacobson 2001; Ramanathan and Carmichael 2008). A number of studies (e.g. Ramanathan et al. 2001; Menon et al. 2002; Randles and Ramaswamy 2008; Ming et al. 2010; Andrews et al. 2010) have shown that they may also alter the hydrological cycle, especially on the regional scale. A sound understanding of absorbing aerosol climate impacts is of great importance, both for attributing past climate change and for projecting future climate change. However, many of the physical and chemical processes involved in the complex interactions among absorbing aerosols, clouds, and climate remain poorly characterized, and are not yet well represented in general circulation models (GCMs) (see Koch and Del Genio (2010) for a comprehensive review).

A particularly acute issue is how to devise a measure of the radiative perturbation to the climate system by absorbing aerosols that both (1) is a good predictor of the response and (2) does not rely heavily on the specifics of model physics parameterization (e.g. Forster et al. 1997; Joshi et al. 2003; Hansen et al. 2005). Several approaches to quantifying the radiative effects of climate change agents have been proposed (Forster et al. 2007). Among them are the instantaneous forcing (IF), which is defined as the change in radiative flux at the tropopause with the atmospheric state held fixed, and the radiative flux perturbation (RFP, also known as fixed-sea surface temperature (SST) forcing), which is defined as the change in radiative flux at the top of the atmosphere (TOA) after atmospheric adjustment, while keeping SST unchanged (Hansen et al. 2005; Haywood et al. 2009). Because it is virtually

independent of often underconstrained model physics parametrization, IF can be compared across different models to assess its accuracy. However, it is a poor indicator of the global-mean surface temperature change (δT_s) caused by absorbing aerosols. Hansen et al. (2005) conducted experiments comparing different forcing calculations for uniform black carbon (BC, a strongly absorbing aerosol in SW) at several layers throughout the troposphere in a NASA GISS GCM, and found that instantaneous forcing is "entirely misleading as a predictor of climate response" for BC, indicating the need for a different method of forcing calculation to efficiently capture the climate response to absorbing aerosols.

In contrast, Hansen et al. (2005) found that one can project δT_s accurately from RFP (or fixed-SST forcing, as it is termed in that paper). RFP has similarly been shown to be an excellent predictor of δT_s for the model used here (Ming et al. 2010). Yet, by allowing the atmosphere to adjust to the initial perturbation, RFP may be prone to uncertainties in parameterized physics (e.g., moist convection, large-scale cloud, and boundary layer schemes), thus rendering it unfit for model inter-comparison (Lohmann et al. 2009).

This study seeks to add clarity to the robustness (or lack thereof) of RFP by identifying the key physical processes underlying the tropospheric response to absorbing aerosols, simulated with an atmospheric GCM. The robustness of a model's RFP value will be dependent on the realism of its representation of aerosol/cloud interactions in the troposphere (Lohmann et al. 2009). A full range of GCMs must be analyzed in order to make a general statement on the robustness of using RFP as a universal quantification of BC forcing, and we here provide such an analysis for the atmospheric component of the Geophysical Fluid Dynamics Laboratory (GFDL) CM2.1 GCM—one the IPCC AR4 models in which the tropospheric response to BC has not yet been analyzed in the context of RFP.

We focus on the Tropics (30°S-30°N), where the climate effects of absorbing aerosols are likely to be particularly strong for at least two reasons. First, the atmospheric burden of absorbing aerosols is relatively high in the Tropics as a result of agricultural biomass burning (Ramanathan and Carmichael 2008). Second, insolation is strongest in the Tropics, which tends to "magnify" the shortwave (SW) radiative effect of a given increase in aerosol burden. The Tropics warrant separate analysis from the extratropics, additionally, since the extratropical response will exhibit significantly more seasonality than the Tropics and is likely to be subject to a very different system of interactions. Thus, while the extratropical response may also be important, it warrants separate investigation from the Tropical analysis presented here.

2. Methodology

The atmospheric GCM simulations used in this study are the same as the atmosphere-only runs used for evaluating RFP in Ming et al. (2010). The model is a modified version of the GFDL AM2.1 atmospheric GCM (The GFDL Global Atmospheric Model Development Team 2004) that includes a prognostic treatment of aerosol-liquid cloud interactions and associated indirect effects (Ming et al. 2006, 2007). It has been used to study the thermal and hydrological responses to different aerosol effects as well as greenhouse gases (Ming and Ramaswamy 2009; Ming et al. 2010). All simulations in this study are forced with climatological SST and sea ice. We perturb a pre-industrial control case with a globally uniform increase in the burden of black carbon of 2.5×10^{-6} kg m^{-2}, all of which is inserted at a specific σ-layer. This burden is chosen to yield a global-mean TOA radiative perturbation

comparable to that of pre-industrial-to-present-day changes in black carbon (approximately 0.53 W m^{-2} in AM2.1 (Ming et al. 2010)), though the spatial distribution (being homogeneous) is not designed to reflect present-day burdens. Given limited knowledge of realistic, present-day horizontal and vertical distributions of BC, such highly idealized experiments are useful for gaining a general understanding of the underlying interactions. We examine the tropospheric responses to the same BC burden located at four layers either in the planetary boundary layer or in the free troposphere (Table 1). Given the strong dependence of BC climate interactions on altitude of emplacement (e.g. Hansen et al. 2005; Erlick et al. 2006), the use of these idealized distributions of BC allows us to systematically develop a conception of how the tropospheric adjustment varies with the altitude of BC in different climate regimes.

3. Results

Figure 1 and Table 1 demonstrate that RFP values and spatial structure diverge strongly from those of IF for BC at all altitudes, and that the vertical location of the BC burden has a strong influence on the global-mean all-sky IF and RFP (incoming/downward radiative flux defined as positive). IF increases monotonically by almost 8 times when the BC layer shifts from immediately above the surface (σ=0.99) to the mid-troposphere (σ=0.60). This is due to the increasingly bright cloud background that is masked by the BC layer (as viewed from TOA) as it rises above more reflective clouds. This cloud-masking phenomenon also explains why only the cloudy-sky component of the IF varies with altitude. In stark contrast, RFP does not correlate with altitude. It shows relatively little variation when BC resides in the

free troposphere (1.2 W m^{-2} for the layer with σ=0.77, and 1.6 W m^{-2} for σ=0.60), and both values are substantially smaller than their respective IF. However, RFP of BC located at σ=0.90, which is typically within the boundary layer, is almost 3 times the corresponding IF. These results indicate that the tropospheric adjustment in response to absorbing aerosols can substantially alter global-mean TOA radiative fluxes. Tropical-mean values for RFP and IF are comparable to global-mean values for all layers (not shown). This indicates that extratropical-mean values will also be comparable to global-mean values, confirming that the extratropical response warrants separate further investigation. We show global-mean values here to facilitate our discussion of energy-balance constraints.

The spatial structure of the RFP due to BC is also strongly tied to the preexisting circulation regime. Thermally driven Tropical circulation is manifested as strong large-scale ascent over the convective regions, which are often in the deep Tropics (5°S-5°N), and compensating subsidence over the vast subtropical regions. As discussed later, the main physical mechanisms driving the tropospheric adjustment differ between these two regimes. We will focus on the West Pacific Warm Pool (WPWP, 10°S-10°N and 90°-150°E) and South Pacific Subsidence Region (SPSR, 30°-5°S and 80°-115°W) to illustrate this point.

a. Mid-tropospheric BC

For mid-tropospheric BC (σ=0.60), the positive IF is generally uniform throughout the Tropics, albeit not without subtle regional differences (Fig. 1(a)). Conversely, IF is relatively weak over the convective regions (e.g., WPWP) due to less low cloud coverage and associated masking. The spatial distribution of RFP, meanwhile, differs dramatically from that of IF

and can (by definition) be attributed to the tropospheric adjustment. The pattern of forcing over the SPSR and other subsidence regions does not differ drastically between IF and RFP. Over the WPWP, however, the local tropospheric adjustment turns the positive IF into a negative RFP, which amounts to a reduction of $\sim$10 W m^{-2} in the net TOA SW absorption. Further analysis indicates that the flux change results exclusively from an increase in SW cloud reflection, leading one to infer that the root cause lies in the impact of BC on cloud formation. This is supported by the large increase in middle cloud amount (cloud top pressure between 440 and 680 hPa) in the WPWP (Fig. 1(c)). The low and high clouds are minimally changed.

What processes then give rise to the increase in middle clouds? BC exerts a local heating of the atmosphere by absorbing incoming SW radiation, as the change in vertical temperature profile shows (Fig. 2(a)). The warming is strongest at 600 hPa where the BC layer roughly lies, and decreases gradually towards the surface. This tends to stabilize the lower free troposphere and hinder the vertical development of moist convection by reducing the convective available potential energy (CAPE). This effect is responsible for the significant decrease in convective mass flux (M_c) at 500 - 600 hPa (Fig. 2(b)). M_c at the top of the boundary layer (approximately 800 - 900 hPa), meanwhile, is dictated largely by the overall atmospheric energy balance (Held and Soden 2006; Ming et al. 2010), and cannot vary nearly as much as at higher altitudes. This enhances the deceleration and detrainment of convective mass into the large-scale environment near 550 hPa, giving rise to a substantial increase in lateral cloud extent (Fig. 2(c)).

While this dynamical effect can explain the overall increase in middle cloud, the vertical structure of the tropospheric response requires further analysis. Following the above line of

7

thinking, one would anticipate cloud cover to decrease above 500 hPa. However, the simulated change in high cloud amount is negligible. Also, despite a downward propagation of warming, the levels above 600 hPa see little variation in temperature. An analysis of the changes in heating rates offers insights into these features of the upper tropospheric response (Fig. 2(d)). The rate of convective heating, realized through compensating subsidence, is equal to $gM_c\partial\theta/\partial p$, where g is the gravitational constant, θ is potential temperature, and p is air pressure. The reduction in M_c at 600 hPa outweighs the increase in local static stability ($\partial\theta/\partial p$), resulting in a decrease in convective heating, which is the main conservation-of-energy mechanism for offsetting the SW heating forced by BC. For the layers below 600 hPa, meanwhile, the latter ($\delta(\partial\theta/\partial p)$) dominates the former ($\delta M_c$), and the associated convective heating contributes to higher local temperature, explaining the observed asymmetry in temperature structure.

This energy balance analysis can be extended to explain the absence of an expected decrease in higher cloud cover. The decrease in convective heating seen at 600 hPa extends well into the upper troposphere mostly due to lower M_c. In the absence of local BC forcing, the latent heat released through large-scale cloud formation increases to balance the weaker convective heating (Fig. 2(d)). As shown in Fig. 2(e), water vapor in the upper troposphere is replenished mainly by advection (dynamics). Since large-scale motion (ω; descent defined as positive) does not vary much with pressure at 300 - 500 hPa, the transport rate can be written as $\omega\partial q/\partial p$, where q is the mass mixing ratio of water vapor. Despite a local warming of $\sim$2 K at 600 hPa, the increase in the upper troposphere temperature is rather limited (typically less than 0.5 K). As the relative humidity remains approximately constant (not shown), q increases with air temperature by 7% K^{-1} (according to the Clausius-Clapeyron

relationship). Thus, the stronger vertical temperature gradient ($\partial T/\partial p$) has an effect of enhancing water vapor advection. This process also adds to cloud cover, thus maintaining the high cloud amount despite the underlying BC-induced detrainment.

b. *Boundary layer BC*

The tropospheric response to boundary layer BC features large reductions in low cloud amount (of up to 10% in absolute value) both over WPWP and over SPSR (Fig. 3(c)). The resulting decrease in cloud reflection greatly amplifies RFP (Fig. 3(b)), which is nearly three times as much as IF in terms of global-means. As discussed previously, IF of BC increases with altitude as a result of brighter background. At σ=0.90, BC is sufficiently close to the surface that IF is negative over the convective regions, where low cloud cover is significantly less than over the subsidence regions (Fig. 3(a)).

Despite a smaller amount of baseline low cloud cover, however, the WPWP does see a reduction in low cloud similar to that seen in the subsidence regions, which can be attributed to the reduced convective entrainment required to balance BC-induced shortwave heating. The model atmosphere reaches a new equilibrium state, in which the SW heating caused by BC is balanced almost entirely by decreased convective heating over WPWP (not shown). Unlike the mid-tropospheric case, the largest reduction in convective mass flux does not take place where the external forcing is (900 hPa), but rather at 950 hPa. As explained before, this is due to the constraint posed by atmospheric energy balance on the convective mass flux out of the boundary layer (Ming et al. 2010). This vertical structure of the change in M_c leads to a substantial reduction in convective detrainment between 950 hPa and the top of

the boundary layer. The large-scale cloud scheme used in this model (Tiedtke 1993) dictates that convective detrainment, rather than large-scale ascent, is responsible for most of the cloud cover over the WPWP. Unsurprisingly, therefore, the weaker convective entrainment necessary for reduced convective heating within the boundary layer results in less low clouds.

Over the subsidence regions, meanwhile, the cloud top BC heating affects boundary layer structure both thermodynamically and dynamically. The vertical profile of potential temperature demonstrates that the top of the well-mixed boundary layer over SPSR is approximately at 900 hPa. A warming of 1.2 K at 900 hPa collocates with a reduction in relative humidity of 10% (12.5% in relative difference) (Figs. 4(a) and (b)). The saturated water vapor pressure increases with temperature roughly at a rate of $7\% \, \mathrm{K}^{-1}$ (the Clausius-Clapeyron relationship). Thus, if the ambient water vapor pressure is unchanged, the warming would cause relative humidity to drop by $\sim$8%. This response is encouragingly consistent with the "semi-direct effect" (Hansen et al. 1997) seen in other GCMs (e.g. Hansen et al. 2005) and corroborated by observations (Ackerman et al. 2000) and large eddy simulations (Johnson et al. 2004). However, this thermodynamic effect alone is not enough to explain all of the simulated drying. The same warming also renders the boundary layer more stable and lowers its top. This dynamical effect, which tends to dry the cloud top by incorporating it into the free troposphere, is responsible for the rest of the simulated drying. As shown in Fig. 4(c), this thermodynamic and dynamical drying and lowering of the boundary layer top lead to a substantial reduction in cloud amount.

The change in cloud amount in the SPSR, however, does not manifest solely at cloud top. Also evident from Fig. 4(c) is a pronounced increase in cloud amount at the layers ($\sim$930 - 960 hPa) that roughly constitute the cloud bottom in the control simulation, an indication

of a lower lifted condensation level (LCL). One can attribute this to higher relative humidity in the lower part of the boundary layer (Fig. 4(b)). Evenly distributed by turbulent diffusion within the boundary layer, the abundance of water vapor is controlled by surface evaporation and cloud top entrainment of dry free troposphere air. While surface evaporation does not vary much in AGCM experiments forced with prescribed SST, such as those studied here, the reduced cloud top LW cooling resultant from a lower cloud top weakens entrainment with an effect of moistening the boundary layer. Overall, however, the cloud top thinning caused by reduced relative humidity outweighs the cloud bottom thickening, resulting in an overall reduction in cloud cover. These results provide insights into the physical mechanisms behind the decrease in low cloud amount (Fig. 3(c)) and, consequently, outgoing SW radiation under RFP.

It is also important to investigate the robustness of the model's mechanism for reestablishing energy balance in the presence of the BC-induced SW heating. The boundary layer top warming tends to weaken turbulent diffusion of heat by stabilizing the boundary layer. Nonetheless, it is still somewhat counterintuitive for the BC-induced SW heating at 900 hPa to be offset mainly by weaker turbulent diffusion, as opposed to LW cooling, especially in light of the rather strong local warming (1.2 K) (Fig. 4(a)). An important factor for determining LW radiation is the lowering of the cloud layer, which results in an increase in LW emissivity (ε) below 900 hPa and a decrease above. For the same temperature profile, an increase (decrease) in ε merely amplifies (damps) local LW cooling. This explains why LW cooling is enhanced below 900 hPa, but becomes weaker (resulting in a net warming) above. At 900 hPa, the impacts of reduced ε and higher temperature approximately balance out each other, with no appreciable change in LW radiation.

11

An analysis of the model's treatment of boundary layer dynamics is also helpful in establishing the robustness of its response to boundary layer BC. Although boundary layer clouds are generally not efficient in generating surface precipitation, the latent heat release from rain formation (condensation) within clouds and subsequent evaporation of falling raindrops below clouds have a stabilizing effect on the boundary layer (Wood 2007). Since both processes, namely cloud condensation and below-cloud evaporation, are represented explicitly by the large-scale cloud scheme in this GCM, a manifestation of this effect is indeed present in the control simulation (not shown). As expected, the large-scale condensational heating shifts downward with the cloud layer (Fig. 4(d)). The change in below-cloud evaporation is almost negligible. The supply of moisture by turbulent diffusion is cut significantly as the boundary layer becomes more stable (Fig. 4(e)), a pattern consistent with decreased cloud amount. The induced BC heating also acts to suppress shallow convection, and weakens the large-scale subsidence (Fig. 4(f)).

4. Discussion

As a system built to be constrained by conservation laws, the GCM's response to the BC forcing can be analyzed in terms of how the model attempts to reestablish energetic equilibrium. Thus, a good starting point for rationalizing the tropospheric adjustments to absorbing aerosols and their radiative consequences at TOA (i.e., the difference between IF and RFP) is to understand how the atmosphere manages to regain energy balance by offsetting the BC-forced SW heating. In doing so, the model is essentially attempting to move the excess energy out of the atmosphere–cross-boundary transport that must take

place at TOA and/or the surface. We begin our analysis of the model's robustness from the perspective of its reequilibrative mechanisms and their associated effects. We feel that this energetics perspective is not fully appreciated in the literature, and could be utilized more in future studies.

Interestingly, the direction that the model system uses to dissipate the BC-induced SW heating is not immediately intuitive, but proves robust. At least in theory, a reduction in atmospheric SW absorption by other agents can accomplish the task of offsetting the BC-induced shortwave absorption. However, the fact that the divergence between TOA and surface IF, which is effectively a measure of the BC-induced heating, is sufficiently close to its RFP counterpart suggests that the SW absorption by non-BC species, mostly likely water vapor, is to the first order unaffected by RFP's tropospheric adjustments (Table 1). The variations in outgoing longwave radiation (OLR) also do not offset the BC perturbation, as they are generally less than 1 W m^{-2} compared to the forced heating (6 - 8 W m^{-2}) (Table 1). This is because of the relatively small change in the stratospheric and upper temperature.

This clearly suggests that instead of being emitted back to outer space, most of the excess heat is deposited to the oceans, which serve effectively as a heat reservoir in prescribed SST experiments. This energy transfer from the atmosphere to oceans is realized in three ways: (1) the lower tropospheric warming strengthens surface downward LW radiation, and the (2) surface sensible and (3) latent heat fluxes into the atmosphere are smaller as well (Table 1). Further analysis reveals that, except for the BC layer immediately adjacent to the surface, the reduction in latent heating is the main mechanism for re-establishing atmospheric energy balance, offsetting about two thirds of the induced heating.

13

This result, albeit somewhat intuitive in light of the critical role of latent heating in maintaining radiative-convective equilibrium, has important implications for the hydrological cycle and general circulation. When coupled with a mixed-layer ocean, the model indicates that the global-mean precipitation, which scales with total latent heating, decreases by 7 - 9% in response to the direct BC heating (Ming et al. 2010). Note that this is an atmosphere-only and thus fast adjustment (Andrews et al. 2010). Since the change in precipitation is much more structured spatially than that in evaporation, it is accompanied by a reduction in low-level moisture (and flow) convergence (i.e., a net divergence). This is consistent with a modest decrease in convective mass flux (M_c) (comparable to the relative change in precipitation) at the boundary layer top (approximately 800 - 900 hPa) as convection is the main means of boundary layer ventilation. In other words, M_c out of the boundary layer is constrained by the overall atmospheric energy balance. In contrast, M_c in the free troposphere is controlled mainly by local energy balance.

In addition to an analysis of the overarching energy balance response to BC throughout the troposphere, subtleties of the model's response to specific BC layers are also of interest. For mid-tropospheric BC, the picture is deceptively simple when BC resides in the subsiding free troposphere. The large-scale subsidence weakens somewhat to offset the forced heating, but without altering the basic characteristics of the underlying circulation regime (i.e., warm, dry and cloud-free). However, the local weaker descent has to be compensated by weaker ascent elsewhere. This means that the BC-induced heating imposed over the subsidence regions can be transported by the large-scale circulation to the convergence zones, where convective adjustment is effective at moving the excess energy out of the atmosphere. A suppression of convection, as is necessary for balancing the dynamical heating, would alter

14

large-scale clouds in ways presumably similar to those discussed above.

For boundary layer BC, the interaction between BC-induced heating and turbulent diffusion, discussed previously in section 3b, is of particular interest. From the viewpoint of energy balance, turbulent transport of sensible heat is critical for sustaining the strong cloud top LW cooling. Thus, it is reasonable to expect that the BC-induced boundary layer heating would be removed by adjusting the turbulent flux of heat. This is confirmed by our model simulation, which indicates clearly that a reduction in turbulent heating plays a central role in re-establishing energy balance (Fig. 4(d)). If one takes the simple view of turbulent diffusion of heat, and assumes unchanged turbulent diffusivity, the vertical profile of temperature change cannot deviate much from the simulated one (Fig. 4(a)). Specifically, the warming peaks at the altitude of the heating source, and decreases gradually both upward and downward. The vertical extent of the warming is limited only by that of turbulent diffusion itself. The temperature of the layers immediately adjacent to the surface is controlled more tightly by strong surface heat flux, and thus is little changed. It is apparent that this pattern would stabilize (destabilize) the layers below (above) the maximum warming, and alter the vertical structure of turbulent diffusivity accordingly. However, such a process should not alter the basic structure of the warming.

Although our model runs do not reflect anthropogenic aerosol distributions, it is possible to consider the modeled effects on M_c in the context of a realistic BC aerosol distribution. The relative decreases in response to a forced increase in SW heating rate at a particular layer $(\delta(\frac{dT}{dt}|_{SW}))$ can be approximated as $\delta(\frac{dT}{dt}|_{SW})/\frac{dT}{dt}|_{CV}$, where $\frac{dT}{dt}|_{CV}$ is the convective heating rate at the same layer in the control case. While $\frac{dT}{dt}|_{CV}$ is spread relatively evenly throughout the free troposphere, anthropogenic BC resides mainly in the lower troposphere as a result of

its short lifetime. As such, the negative buoyancy generated by realistic BC-induced heating may reduce M_c even further as it rises above the boundary top, giving rise to more detrained large-scale clouds. Even though this effect is somewhat exaggerated in our mid-tropospheric BC case, as all the forcing is concentrated within a single layer, the physical argument laid out here leads one to expect it to be robust, at least qualitatively, for any reasonably simulated ("bottom-heavy") distribution of anthropogenic absorbing aerosols. Care should be taken, however, when attempting to compare layer-dependent idealizations such as this one with realistic distributions, as it is unclear whether the response for different altitudes of idealized BC emplacement will be linearly additive.

5. Conclusion

As one uses GCMs to explore how BC, when intermingled with boundary layer clouds, may alter them, an unavoidable problem is the model's inability to simulate boundary layer clouds realistically, which is an outcome of, among other things, insufficient vertical resolution (too coarse to resolve the sharp inversion) and the intrinsic difficulty in parameterizing turbulent fluxes. Here, we argue that despite these deficiencies, the main characteristics of the GCM-simulated response are qualitatively robust. For boundary layer BC, the significant loss in cloud amount (the so-called "cloud burn-off" or semi-direct effect, demonstrated first by Hansen et al. (1997)) is largely the consequence of the thermal response, both thermodynamically and dynamically manifested. It is entirely possible that a GCM with different boundary layer and large-scale cloud schemes may yield quantitatively different answers, but the expectation is that the effect's overall sign and main mechanisms are robust regardless

16

of model physics. For free tropospheric BC, the increase in middle cloud caused predominantly by changing M_c can be robustly justified via the convective heating energy balance necessitated by BC-induced SW heating.

The failure of IF to accurately predict δT_s caused by absorbing aerosols makes it particularly important to find a reasonable substitute. As shown in this study, absorbing aerosols are capable of affecting cloud cover through both thermodynamic and dynamical processes with significant impacts on cloud distribution and TOA radiative fluxes. We conclude that the sources of the largest differences between IF and RFP in the Tropics are derived from theoretically sound physical mechanisms rather than model artifacts. Though only the Tropics are here analyzed, the extratropics may also have a significant contribution to the RFP value. One can expect, however, that the Tropical regime will be similar to that of extratropical summer, with the extratropical land behaving much like the Tropical convective regions and the extratropical ocean behaving much like the subtropical subsidence regions. The extratropical winter response, however, is likely to operate under very different conditions and warrants further investigation. The physical explanations for the Tropical tropospheric response given here, however, suggest that RFP is a generally robust (i.e. attributable to sound physics) and representative (i.e. well-correlated with δT_s) forcing calculation for BC in this model, lending support to the argument that RFP can serve as an accurate yet robust alternative for quantifying the potential of absorbing aerosols to modify the climate.

17

Philip Stier, Simon Klemperer, and Ken Caldeira for research guidance. G.P. was supported during the initial phase of research by the Ernest F. Hollings Undergraduate Scholarship Program, administered by NOAA's Office of Education.

REFERENCES

Ackerman, A. S., O. B. Toon, D. E. Stevens, A. J. Heymsfield, V. Ramanathan, and E. J. Welton, 2000: Reduction of tropical cloud cover by soot. *Science*, **288**, 1042–1047.

Andrews, T., P. M. Forster, O. Boucher, N. Bellouin, and A. Jones, 2010: Precipitation, radiative forcing and global temperature change. *Geophys. Res. Lett.*, **37**, doi:10.1029/2010GL043991.

Erlick, C., V. Ramaswamy, and L. M. Russell, 2006: Differing regional responses to a perturbation in solar cloud absorption in the skyhi general circulation model. *J. Geophys. Res.*, **111**.

Forster, P., et al., 2007: Changes in atmospheric constituents and in radiative forcing. *Climate Change 2007: The Physical Science Basis. Contribution of Working Group I to the Fourth Assessment Report of the Intergovernmental Panel on Climate Change*, S. Solomon, D. Qin, M. Manning, Z. Chen, M. Marquis, K. B. Averyt, M. Tignor, and H. L. Miller, Eds., Cambridge University Press, Cambridge, United Kingdom and New York, NY, USA.

Forster, P. M. F., R. S. Freckleton, and K. P. Shine, 1997: On aspects of the concept of radiative forcing. *Climate Dyn.*, **13**, 547–560.

Hansen, J., M. Sato, and R. Ruedy, 1997: Radiative forcing and climate response. *J. Geophys. Res.*, **102**, 6831?–6864.

Hansen, J., M. Sato, R. Ruedy, A. Lacis, and V. Oinas, 2000: Global warming in the twenty-first century: An alternative scenario. *J. Geophys. Res.*, **97**, 9875–9880.

Hansen, J., et al., 2005: Efficacy of climate forcings. *J. Geophys. Res.*, **110**, doi:10.1029/2005JD005776.

Haywood, J. M., L. J. Donner, A. Jones, and J.-C. Golaz, 2009: Global indirect radiative forcing caused by aerosols: IPCC (2007) and beyond. *Clouds in the Perturbed Climate System*, J. Heintzenberg and R. Charlson, Eds., MIT Press, Cambridge, MA, USA.

Held, I. M. and B. J. Soden, 2006: Robust responses of the hydrological cycle to global warming. *J. Climate*, **19**, 5686–5699.

Jacobson, M. Z., 2001: Strong radiative heating due to the mixing state of black carbon in atmospheric aerosols. *Nature*, **409**, 695–697.

Johnson, B. T., K. P. Shine, and P. M. Forster, 2004: The semi-direct aerosol effect: Impact of absorbing aerosols on marine stratocumulus. *Q. J. R. Meteorol. Soc.*, **130**, 1407–1422.

Joshi, M., K. Shine, M. Ponater, N. Stuber, R. Sausen, and L. Li, 2003: A comparison of climate response to different radiative forcings in three general circulation models: Towards an improved metric of climate change. *Climate Dyn.*, **20**, 843–854.

Koch, D. and A. Del Genio, 2010: Black carbon absorption effects on cloud cover, review and synthesis. *Atmos. Chem. Phys. Discuss.*, **10**, 7323?7346.

Lohmann, U., et al., 2009: Total aerosol effect: radiative forcing or radiative flux perturbation? *Atmos. Chem. Phys. Discuss.*, **9**.

Menon, S., J. Hansen, L. Nazarenko, and Y. Lao, 2002: Climate effects of black carbon aerosols in China and India. *Science*, **297**, 2250–2253.

Ming, Y. and V. Ramaswamy, 2009: Nonlinear climate and hydrological responses to aerosol effects. *J. Climate*, **22**, 1329–1339.

Ming, Y., V. Ramaswamy, L. J. Donner, and V. T. J. Phillips, 2006: A new parameterization of cloud droplet activation applicable to general circulation models. *J. Atmos. Sci.*, **63**, 1348–1356.

Ming, Y., V. Ramaswamy, L. J. Donner, V. T. J. Phillips, S. A. Klein, P. A. Ginoux, , and L. W. Horowitz, 2007: Modeling the interactions between aerosols and liquid water clouds with a self-consistent cloud scheme in a general circulation model. *J. Atmos. Sci.*, **64**, 1189–1209.

Ming, Y., V. Ramaswamy, and G. Persad, 2010: Two opposing effects of absorbing aerosols on global-mean precipitation. *Geophys. Res. Lett.*, **37**, doi:10.1029/2010GL042895.

Ramanathan, V. and G. Carmichael, 2008: Global and regional climate changes due to black carbon. *Nature Geosci.*, **1**, 221–227.

Ramanathan, V., P. J. Crutzen, J. T. Kiehl, and D. Rosenfeld, 2001: Aerosols, climate, and the hydrological cycle. *Science*, **294**, 2119–2124.

Randles, C. and V. Ramaswamy, 2008: Absorbing aerosols over Asia: A Geophysical Fluid Dynamics Laboratory general circulation model sensitivity study of model response to aerosol optical depth and aerosol absorption. *J. Geophys. Res.*, **113**, doi: 10.1029/2008JD010140.

The GFDL Global Atmospheric Model Development Team, 2004: The new GFDL global atmosphere and land model AM2-LM2: Evaluation with prescribed SST simulations. *J. Climate*, **17**, 4641–4673.

Tiedtke, M., 1993: Representation of clouds in large-scale models. *Mon. Wea. Rev.*, **121**, 3040–3061.

Wood, R., 2007: Cancellation of aerosol indirect effects in marine stratocumulus through cloud thinning. *J. Atmos. Sci.*, **64**, 2657–2669.

List of Tables

TABLE 1. Global-mean TOA and surface instantaneous forcing (IF) and radiative flux perturbation (RFP) (downward defined as positive), changes in surface latent and sensible heat fluxes into the atmosphere (LH and SH, respectively) for BC inserted at different σ-layers, with their approximate altitudes in meters in parentheses. IF is entirely in SW, while the SW and LW components of TOA and surface RFP are given in parentheses.

σ (altitude)	TOA IF	surface IF	TOA RFP	surface RFP	LH	SH
0.99 (35)	0.48	-5.7	0.92 (1.6, -0.68)	-3.9 (-4.7, 0.8)	-0.58	-3.9
0.90 (850)	1.1	-5.0	3.2 (3.9, -0.72)	-2.6 (-3.1, 0.50)	-4.3	-1.4
0.77 (2200)	2.8	-6.0	1.2 (1.9, -0.63)	-5.0 (-7.3, 2.3)	-4.7	-1.4
0.60 (4100)	3.9	-6.0	1.6 (1.2, 0.39)	-6.4 (-8.9, 2.5)	-6.4	-1.3

24

List of Figures

4   Vertical distributions of the changes in (a) temperature (K), (b) relative humidity (%), (c) cloud amount (%) , (d) heating rates (10^{-5} K s^{-1}), (e) tendencies in water vapor mass mixing ratio (10^{-9} kg kg^{-1} s^{-1}), and (f) large-scale motion (10^{-3} Pa s^{-1}) and convective mass flux (10^{-3} kg m^{-2} s^{-1}) over SPSR due to boundary layer black carbon (σ=0.90). The abbreviations are SW (shortwave), LW (longwave), CV (convection), LS (large-scale), VD (vertical diffusion) and DY (dynamical). The y-axis is pressure in hPa.   30
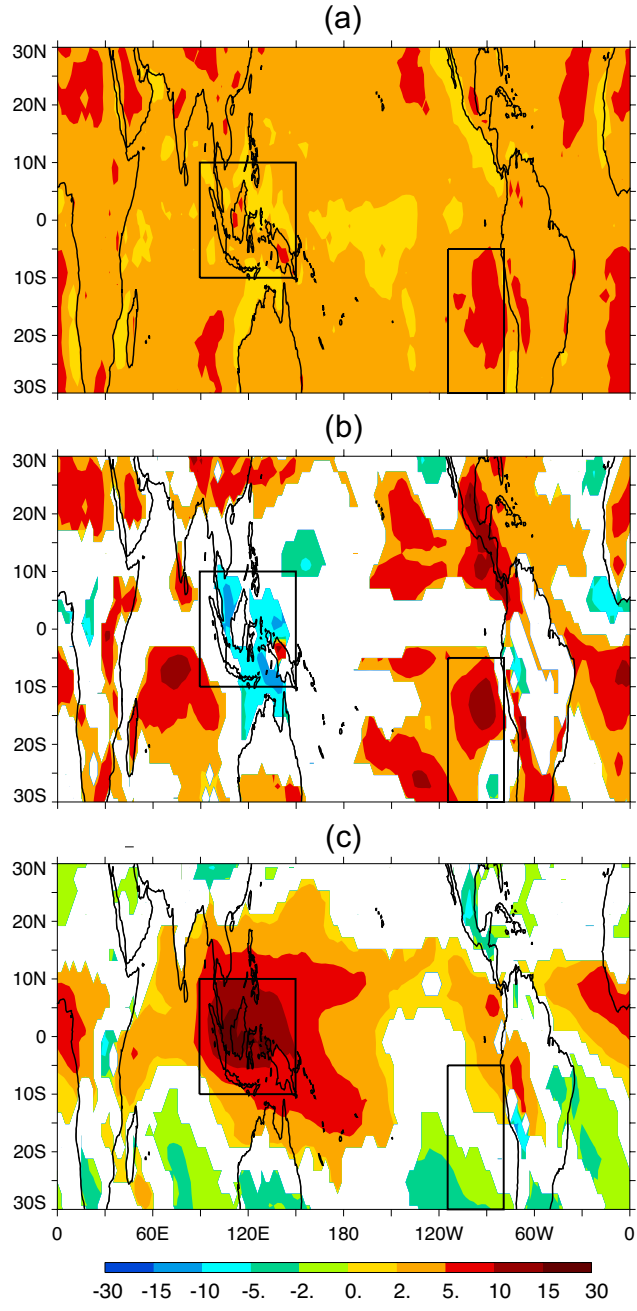
FIG. 1. Annual-mean (a) instantaneous forcing (W m^{-2}), (b) radiative flux perturbation (W m^{-2}) and (c) change in middle cloud amount (%) due to mid-tropospheric black carbon (σ=0.60). The rectangular boxes denote the WPWP and SPSR, respectively.
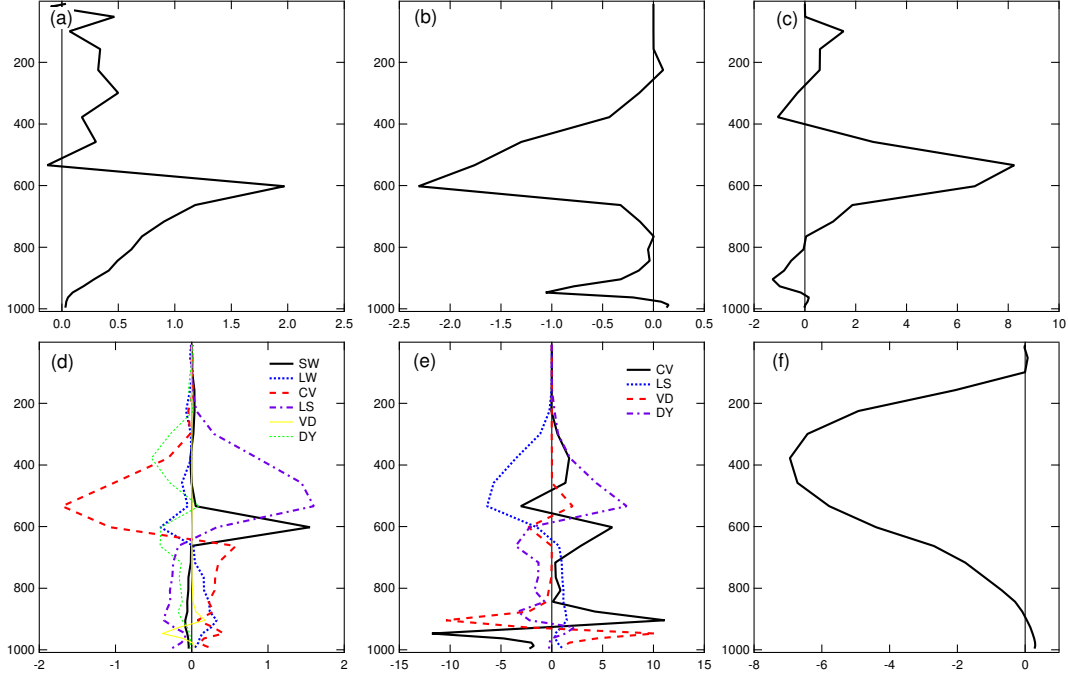
FIG. 2. Vertical distributions of the changes in (a) temperature (K), (b) convective mass flux (10^{-3} kg m^{-2} s^{-1}), (c) cloud amount (%) , (d) heating rates (10^{-5} K s^{-1}), (e) tendencies in water vapor mass mixing ratio (10^{-9} kg kg^{-1} s^{-1}), and (f) large-scale motion (10^{-3} Pa s^{-1}) over the WPWP due to mid-tropospheric black carbon (σ=0.60). The abbreviations are SW (shortwave), LW (longwave), CV (convection), LS (large-scale), VD (vertical diffusion) and DY (dynamical). The y-axis is pressure in hPa.
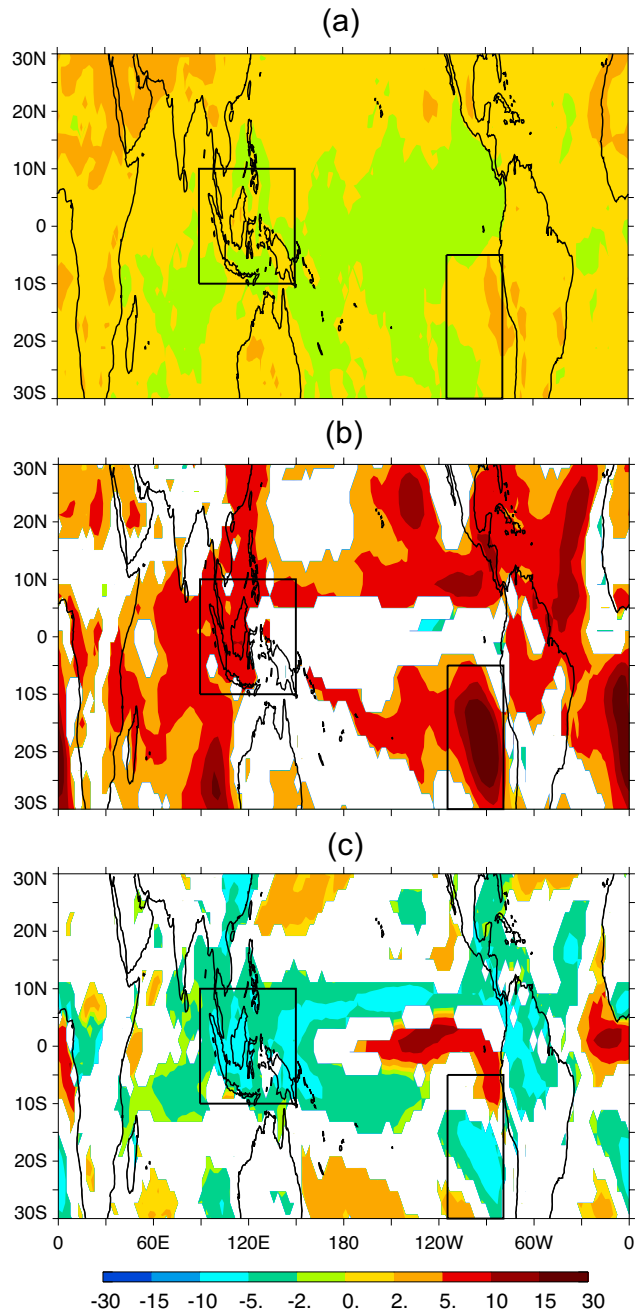
FIG. 3. Annual-mean (a) instantaneous forcing (W m^{-2}), (b) radiative flux perturbation (W m^{-2}) and (c) change in low cloud amount (%) due to boundary layer black carbon (σ=0.90). The rectangular boxes denote the WPWP and SPSR, respectively.
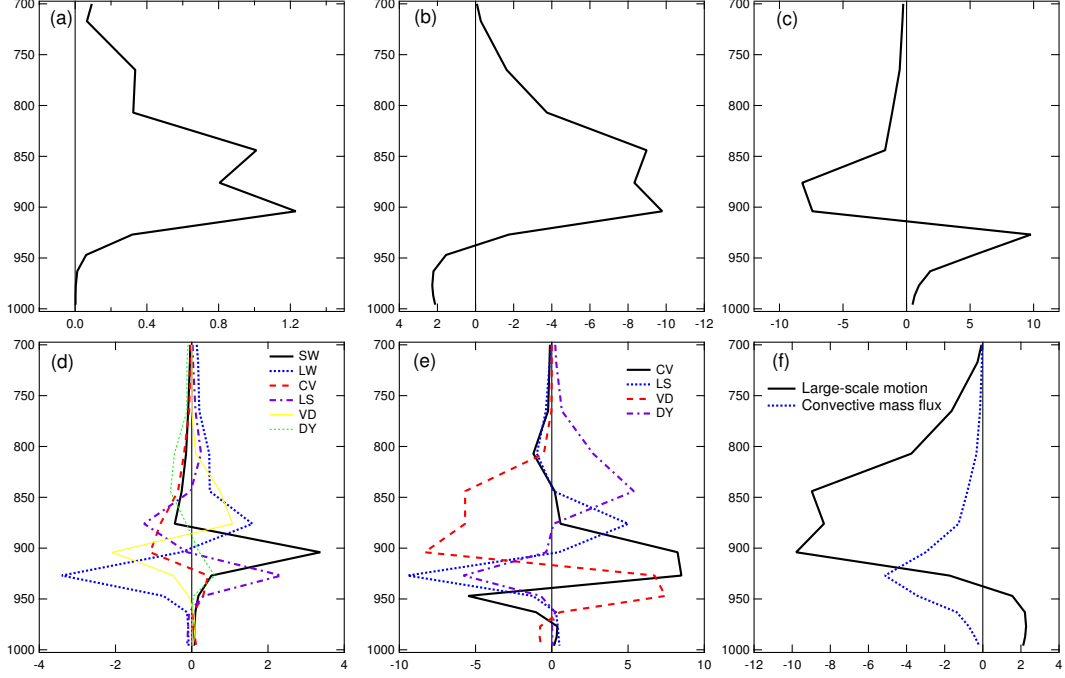
FIG. 4. Vertical distributions of the changes in (a) temperature (K), (b) relative humidity (%), (c) cloud amount (%) , (d) heating rates (10^{-5} K s^{-1}), (e) tendencies in water vapor mass mixing ratio (10^{-9} kg kg^{-1} s^{-1}), and (f) large-scale motion (10^{-3} Pa s^{-1}) and convective mass flux (10^{-3} kg m^{-2} s^{-1}) over the SPSR due to boundary layer black carbon (σ=0.90). The abbreviations are SW (shortwave), LW (longwave), CV (convection), LS (large-scale), VD (vertical diffusion) and DY (dynamical). The y-axis is pressure in hPa.